colloids and interfaces

MDPI

Article

Effects of Cooling Rate and Emulsifier Combination on the Colloidal Stability of Crystalline Dispersions Stabilized by Phospholipids and β-Lactoglobulin

Jasmin Reiner [1,*], Charlotte Schüler [2], Volker Gaukel [1] and Heike Petra Karbstein [1]

[1] Karlsruhe Institute of Technology, Institute of Process Engineering in Life Sciences—Food Process Engineering, 76131 Karlsruhe, Germany; volker.gaukel@kit.edu (V.G.); heike.karbstein@kit.edu (H.P.K.)
[2] Department of Food Technology, Engineering and Nutrition, Lund University, S-22100 Lund, Sweden
* Correspondence: jasmin.reiner@kit.edu

Abstract: A lot of applications for (semi-)crystalline triacylglycerol (TAG)-in-water dispersions exist in the life science and pharmaceutical industries. Unfortunately, during storage, these dispersions are often prone to changes in particle size due to unforeseen crystallization and recrystallization events. This results in the alterations of important product properties, such as viscosity and mouthfeel, or the premature release of encapsulated material. In this study, we investigated the effects and interplay of formulation, i.e., emulsifier combination, and processing parameters, i.e., cooling rate, on the colloidal stability of dispersed TAGs and aimed to improve their colloidal stability. We chose phospholipids (PLs) and β-lactoglobulin (β-lg) as the emulsifiers for our model systems, which are commonly applied in many food systems. When dispersions were characterized directly after cooling, we obtained smaller particles and narrower size distributions after fast cooling. Over the course of eleven weeks, the creaming behavior, particle size, melting behavior and polymorphism were characterized. The dispersions stabilized with solely β-lg exhibited a slight increase in particle size, whereas a decrease in size was found when PLs were added. Our results indicate that mass transport phenomena between TAG droplets and particles took place during storage. This migration of TAG molecules changed the composition and size distribution of the dispersed phase, especially at higher PL concentration (0.1 wt%). In our case, this could be prevented by using a lower concentration of PLs, i.e., 0.05 wt%.

Keywords: phospholipid; β-lactoglobulin; (semi-)crystalline dispersion; triacylglycerol; colloidal stability; polymorphism; mass transport

Citation: Reiner, J.; Schüler, C.; Gaukel, V.; Karbstein, H.P. Effects of Cooling Rate and Emulsifier Combination on the Colloidal Stability of Crystalline Dispersions Stabilized by Phospholipids and β-Lactoglobulin. *Colloids Interfaces* **2023**, *7*, 45. https://doi.org/10.3390/colloids7020045

Academic Editors: Reinhard Miller, Eleni P. Kalogianni and Julia Maldonado-Valderrama

Received: 24 April 2023
Revised: 30 May 2023
Accepted: 31 May 2023
Published: 5 June 2023

1. Introduction

A lot of products in the pharmaceutical and life science industries, e.g., for the encapsulation of lipophilic agents or food products, such as milk, cream or recombined dairy products, consist of emulsified natural fats, which are composed of a wide variety of different triacylglycerols (TAGs) [1–4]. The dispersed phase in these oil-in-water (O/W) dispersions may be (partially) crystalline, depending on the composition and storage temperature, and is kinetically stabilized by low-molecular-weight emulsifiers (LMWEs) such as phospholipids (PLs) and/or proteins, e.g., from whey [5,6]. These dispersions are thermodynamically unstable, where stability is the resistance of systems to physical changes [7]. They may, therefore, undergo creaming, coalescence, aggregation and Ostwald ripening during storage and transport [8–11]. Due to the presence of (partially) crystalline particles, partial coalescence, iso-mass recrystallization and polymorphic transitions may also occur [8,12–16]. All these phenomena lead to alterations of dispersion characteristics, or even to a loss of product functionality and applicability. Therefore, the goal is to suppress these changes through suitable choice of process and formulation parameters. One possibility to slow down or suppress these colloidal instability phenomena is by using

suitable choice of emulsifiers or combinations thereof, such as proteins and LMWEs. They are used in combinations in a wide range of applications or co-occur through their presence in specific ingredients. The stabilization mechanism of PLs and proteins differs due to their molecular nature. Proteins adsorb comparably slowly and many authors have shown that they can unfold at droplet interfaces [17–19]. Lateral interactions between adsorbed molecules may then lead to the creation of a viscoelastic film, which is important for protecting droplets against coalescence [20,21]. Generally, hydrophobic parts of proteins are exposed during unfolding and, thus, adsorb in train conformations, whereas hydrophilic parts protrude from the interface into the continuous phase [20,22]. This can result in a thick interfacial layer of up to 2–3 nm and an extensive steric stability [4]. On the other hand, PLs are LMWEs that can adsorb quickly at the interface [23–25]. Therefore, LMWEs are very efficient in stabilizing newly created, uncovered oil–water interfaces and in displacing proteins from existing interfaces [21,26]. The displacement has been shown to be concentration dependent and more pronounced with water-soluble than with oil-soluble LMWEs. However, a complete displacement of protein has not been observed, even at high phospholipid-to-protein ratios [27]. Furthermore, PLs and proteins can undergo complexation [20]. Such complexes can display surface activity, which can even be more pronounced than that of their individual constituents. Complexing emulsifiers may also undergo structural changes, which alters their characteristics [28,29]. Therefore, we expect enhanced colloidal stability in systems stabilized with combinations of proteins and PLs compared to systems solely stabilized with proteins. This means that instabilities, such as aggregation and (partial) coalescence, will be prevented or occur to a smaller extent over a defined period of time.

LMWEs have also been shown to act as crystallization templates that trigger crystallization in dispersed TAG droplets [30,31]. In general, droplet crystallization is an individual and stochastic process differing from droplet to droplet [30,32]. It occurs over a wide temperature range. Supercooling needed to trigger fat crystallization is higher in droplets than in bulk fat and increases with decreasing droplet size [33,34]. Crystallization is commonly divided into two sub-processes, i.e., nucleation, which is followed by crystal growth. Crystals can only grow after stable nuclei have been formed, for example, via heterogeneous nucleation [4]. In emulsified systems, surface or volume heterogeneous nucleation may promote the formation of nuclei within a droplet. Volume heterogeneous nucleation occurs when catalytic impurities are present in oil droplets. In addition, it has been shown that lipid-based LMWEs can promote surface heterogeneous nucleation in O/W emulsions [35]. During surface heterogeneous nucleation, the tails of lipid-based LMWEs, which are oriented toward the dispersed fat phase in O/W emulsions, can initiate nucleation by conferring a certain degree of order to neighboring TAG molecules [30,31]. Then, LMWEs act as the so-called "templates" for nuclei formation [36,37]. In addition, the crystallization of a LMWE itself can induce TAG nucleation and crystallization of droplets. Proteins, on the other hand, have not been shown to initiate surface heterogeneous nucleation as seen with lipid-based LMWEs [38]. It is assumed this is because their hydrophobic patches lack compatibility with the chemical structure of emulsified TAGs and, thus, they do not get incorporated into compound fat crystals [26]. There is, however, evidence that the degree of supercooling, i.e., the temperature at which droplets are still liquid, can be influenced by the type of protein used as emulsifier. It was reported that emulsions of hydrogenated palm oil showed higher supercooling when stabilized with a mixture of whey proteins and caseins compared to emulsions stabilized with whey proteins alone [39]. Based on this knowledge, we expect that the addition of PLs to protein-based dispersions will lead to protein surface heterogeneous nucleation, thereby increasing the solid fat content of the system and resulting in better colloidal stability of the dispersions. In addition, we assume this effect is more pronounced with a PL with a larger hydrophilic headgroup compared to a PL with a smaller one. This is assumed due to a higher affinity to the interface and stronger protein displacement when using larger headgroups.

After nucleation, crystal growth follows, where TAGs crystallize in different modifications, whereby, in general, a distinction is made between α, β′ and β polymorphs. These modifications can be in double- or triple-layer lamellar structure, depending on the hydrocarbon chain packing [40]. α polymorph is characterized as being hexagonal, β′ is characterized as being orthorhombic perpendicular, and β is characterized by a triclinic parallel subcell [41]. Due to their different molecular packing, the activation energy, thermodynamic stability, packing density, ordering and melting point increase from α to β′ to β form [42,43]. Furthermore, polymorphic transitions may occur during storage, and the transformation of α to β′ and β is irreversible and occurs toward a more hydrodynamic stable system [44]. To differentiate the polymorphic forms and detect polymorphic transitions, X-ray diffraction (XRD) and differential scanning calorimetry (DSC) are routinely used for bulk fats [45–47] and emulsions [12,48,49]. In an emulsion, polymorphic transitions occur earlier during storage than in bulk and the course may be altered [50–52]. Different proportions of α, β′ and β modification exist in emulsions depending on the droplet size and supercooling and cooling rates [4,9,53]. Additionally, the molecular structure of triacylglycerols and LMWEs can influence the formation of different polymorphs and their transitions [54–56]. For instance, it was shown that the addition of PLs with similar molecular structure to the dispersed fat phase led to retarded polymorphic transitions of dispersed TAGs [31]. The reason is believed to be due to the restricted fluidity and mobility of TAG crystals by crystalline PLs at the interface inhibiting crystal rearrangement [31,35]. These polymorphic transitions can promote dispersion destabilization due to the shape changes of solid particles from spherical to ellipsoidal, which often leads to extensive aggregation [9,57]. Therefore, this inhibitory effect of LMWEs on polymorphic transitions is assumed to contribute to improved colloidal stability in dispersions. Moreover, the cooling rate and level of supercooling applied to dispersions are known to influence the nucleation and crystallization behavior of TAG molecules and, thus, affect their crystal polymorphism, size and shape [9,16,58]. High heating and cooling rates have been shown to delay polymorphic transitions and are, therefore, expected to increase colloidal stability against aggregation. We, thus, expect that the combination of fast cooling and addition of PLs to protein-based dispersions will increase their colloidal stability during storage when compared to slow cooling and the use of a sole protein as an emulsifier. Again, we assume increased colloidal stability with a more hydrophilic PL.

Therefore, the goal of this study was to investigate the effect and interplay of formulation and processing parameters on the colloidal stability of dispersed TAGs. It was not the aim of this study to gain mechanistic understanding of interfacial or colloidal phenomena. First, we compared particle morphology and size, as well as viscosity, of different dispersions directly after preparation to obtain information about the influence of formulation and cooling process on dispersion characteristics. We expected smaller particles when PLs were present and a fast cooling rate was applied. Second, based on the hypothesis that the addition of PLs to protein-stabilized emulsified TAGs would improve the overall stability of the emulsion system, we compared colloidal stability against macrostructural and particle size changes and polymorphic transitions between dispersions stabilized solely with β-lactoglobulin and dispersions stabilized with β-lactoglobulin combined with PLs over the course of three months. Third, the influence of the hydrophilic headgroup was investigated via the addition of two phospholipids, phosphatidylcholine (PC) and phosphatidylethanolamine (PE), differing only in their headgroup to the protein-based dispersions. We expected that PC would lead to better colloidal stability over the storage period due to its larger hydrophilic headgroup. Lastly, we decided to manipulate the cooling rate as a processing parameter and investigate the effect of a fast, moderate and slow cooling process on the colloidal stability of TAG dispersions. We expected to obtain the most stable protein-based dispersion when a PL with a large hydrophilic headgroup was added as a co-surfactant and a fast cooling rate was applied.

The findings are supposed to benefit companies that market products with a similar composition to the dispersion system studied here. If the investigated approaches are found to be effective in improving product quality and prolonging storage stability, this would bring obvious economic benefits by increasing the appeal and competitiveness of the products formulated and processed as proposed in this study. An optimized formulation and manufacturing process would also allow companies to save resources and prevent product waste. Even though this study was not intended to gain mechanistic understanding of interfacial or colloidal phenomena, it would add data that may serve to elucidate the molecular interactions of PLs and whey proteins in TAG emulsions.

2. Materials and Methods

2.1. Raw Materials

Softisan® 154 was kindly provided by IOI Oleo GmbH (Hamburg, Germany). It is a hydrogenated palm oil containing mixed TAGs esterified with over 95% 16:0/18:0 FAs and the remaining fraction of 12:0/14:0 FAs. The two phospholipids, LIPOID PC 18:0/18:0 and LIPOID PE 18:0/18:0, were kindly provided by Lipoid GmbH (Ludwigshafen, Germany). They were chosen because they have a similar FA composition but differ in their hydrophilic head group. PC is phosphatidylcholine, whereas PE is phosphatidylethanolamine, which means a choline or an ethanolamine head group is esterified with FAs, respectively. The choline headgroup is larger in size compared to ethanolamine, which accounts for the different geometry of PCs and PEs. While PCs, with their large headgroup, have a morphology of a truncated cone, their hydrophobic moiety dominates over the comparably smaller headgroup in PEs [59]. Additionally, PLs were chosen due to their FA similarity to Softisan® 154, i.e., the degree of saturation and chain length. β-lactoglobulin (β-lg) was purchased from TU Munich (Munich, Germany). Sodium hydroxide (NaOH) was purchased from Carl Roth GmbH + Co. KG (Karlsruhe, Germany), and potassium sorbate was purchased from VWR International (Leuven, Belgium). Water was purified using a MicroPure™ water purification system provided by Thermo Fisher Scientific Inc. (Waltham, MA, USA).

2.2. Emulsion Preparation

The samples were prepared via melt emulsification, producing a coarse premix, which was then processed into a finely dispersed emulsion. To prevent dispersed-phase crystallization during emulsification, the process was carried out at 10 K above the melting temperature of the dispersed phase. All samples consisted of 5 wt% Softisan® 154 as the dispersed phase and 0.5 wt% β-lg as the emulsifier. The two phospholipids, LIPOID PC 18:0/18:0 and LIPOID PE 18:0/18:0, were additionally used as emulsifiers in two different concentrations (0.05 wt% and 0.1 wt%). The composition of the phospholipids used can be found in Table A1. The samples stabilized by β-lg alone serve as the reference (*Ref*), and the samples containing the phospholipids PC and PE are further abbreviated as "*Chol*" and "*Eta*" to accentuate their differing headgroups. The sample names and compositions are given in Table 1.

2.2.1. Preparation of Coarse Emulsion

First, 0.53 wt% β-lg was dissolved in water at room temperature by stirring for 2 h. The water was adjusted to a pH of 6.5 using 1 M NaOH to avoid protein precipitation at its isoelectric point (IEP). The protein solution was then refrigerated overnight to ensure full protein hydration.

The fat and phospholipid fractions were mixed and melted at 85 °C in a water bath for at least 20 min to erase crystal memory of the TAG. Afterwards, the protein solution was added, and a coarse emulsion was prepared using an IKA® T25 digital ULTRA TURRAX tooth-rim dispersing machine (IKA-Werke GmbH & Co. KG, Staufen im Breisgau, Germany) at a tangential speed of 2.5 m/s (3200 rpm, 13 mm rotor outer diameter) for 2 min.

2.2.2. Preparation of Fine Emulsion

The coarse premix was finely dispersed using an IKA® magic LAB® colloid mill (IKA-Werke GmbH & Co. KG, Staufen im Breisgau, Germany) at an average circumferential speed of 36.7 m s^{-1} (25,000 rpm, respectively, with the upper radius of the rotor = 11.5 mm, the lower radius of the rotor = 16.5 mm, and the radial gap = 0.159 mm) for 10 min. The device was preheated by circulating hot water during the operation of the colloid mill. The process temperature was kept constant at 65 °C using a double-walled storage container.

Table 1. Overview of sample names, their composition and cooling procedure.

Sample Name	Cooling Rate	Softisan® 154	β-lg	LIPOID PC 18:0/18:0	LIPOID PE 18:0/18:0
Ref slow	slow	5 wt%	0.5 wt%		
Ref moderate	moderate				
Ref fast	fast				
Chol 0.05 slow	slow	5 wt%	0.5 wt%	0.05 wt%	
Chol 0.05 moderate	moderate				
Chol 0.05 fast	fast				
Chol 0.1 slow	slow	5 wt%	0.5 wt%	0.1 wt%	
Chol 0.1 moderate	moderate				
Chol 0.1 fast	fast				
Eta 0.05 slow	slow	5 wt%	0.5 wt%		0.05 wt%
Eta 0.05 moderate	moderate				
Eta 0.05 fast	fast				
Eta 0.1 slow	slow	5 wt%	0.5 wt%		0.1 wt%
Eta 0.1 moderate	moderate				
Eta 0.1 fast	fast				

Each sample volume was split equally into three glass vials, which were then subjected to three different cooling processes. One vial was cooled at room temperature (RT), and the other two were transferred to a 5 °C refrigerator (RF) and a 0 °C ice bath (IB), respectively, until they reached a final temperature of 22 °C. These cooling conditions were used to mimic slow (RT, 0.01–0.1 K/min), moderate (RF, 0.5 K/min) and fast (IB, 10 K/min) cooling [16]. The applied rate of cooling and the corresponding sample names are summarized in Table 1. Because solid and liquid lipids may exist after the cooling of the samples, they are referred to as "dispersions".

2.2.3. Storage Conditions

After cooling, the dispersions were stored in the dark at a constant temperature of 22 °C, and 0.2 wt% potassium sorbate was added to all samples to prevent spoilage during storage. Whenever a sample aliquot was needed for analysis, the sample container was gently inverted three times to allow a homogeneous sampling process, thereby avoiding excessive mechanical energy input. The pH was checked regularly. In general, measurements were performed over a total period of three months at the following intervals: t_0 = directly after sample preparation, t_2 = after two weeks, t_4 = after four weeks, t_8 = after eight weeks, and t_{11} = after eleven weeks.

2.3. Determination of Mictrostructure

The microstructure of the samples was assessed at room temperature using a polarized light microscope (Eclipse LV100ND, Nikon, Shinagawa, Tokyo, Japan). Polarized light microscopy allows isotropic and anisotropic materials to be distinguished; thus, liquid oil appears non-colored and crystalline fat appears as bright colored structures. Additionally, the size and shape of particles, as well as the changes in the microstructure, were investigated. Both native and diluted (1:10) samples were assessed to study the overall

microstructure, as well as to characterize individual colloidal particles. A total of 10 µL of each sample was pipetted onto an object slide and covered with a cover slip.

2.4. Measurement and Analysis of Particle Size Distribution

The particle size distribution (DSD) of the dispersions was determined via laser diffraction analysis using a HORIBA LA-950V2 (Retsch Technology, Haan, Germany) in a stirred fraction cell. A refractive index of 1.460–0.001i was used. The particle size distribution was determined as a cumulative normalized size distribution based on the particle volume (Q_3). Q_3(x) was used to detect possible (partial) coalescence and flocculation events, which would result in an increase in particle size. As measures of the smallest and largest sizes in the collectives, the x_{10} and x_{90} percentiles were determined based on the particle volume (Q_3). Hence, in the case of volume-based size distribution, $x_{10,3}$ ($x_{90,3}$) is defined as the particle diameter, at which 10% (90%) of the particle volume is represented by particles up to this diameter.

2.5. Rheological Characterization

The dispersion viscosity as a function of the shear rate was measured using a Physica MCR 301 stress-controlled rheometer with a coaxial double-gap geometry DG26.7 (Anton Paar Germany GmbH, Ostfildern-Scharnhausen, Germany). The experiments were carried out at 22 °C with a shear rate ranging from 0.1 to 1000 s^{-1}.

2.6. Creaming Index

The colloidal structure of the dispersions was assessed visually by photographing the samples in a transparent storage container against a black background. The height of the top creamed layer (H_C) and the total dispersion (H_T) were measured using a precision ruler, and the values were used to determine the creaming index (CI) adopted and modified from Zhang et al. [60] according to Equation (1):

$$CI(\%) = 100 \times \frac{H_C}{H_T} \quad (1)$$

2.7. Differential Scanning Calorimetry

The melting behavior of dispersed triacylglycerol was analyzed using a double-furnace differential calorimeter DSC 8500 (Perkin Elmer Inc., Waltham, MA, USA). The calorimeter was calibrated against indium (T_m = 156.6 °C), water (T_m = 0.000 °C) and n-decane (T_m = −29.65 °C) at a scanning rate of ±2.5 K/min. A total of 9–11 mg of the samples was loaded into aluminum pans. The pans were heated to 70 °C at a constant scanning rate of 2.5 K/min. After 5 min holding time, they were cooled back to 22 °C at 20 K/min. The total melting enthalpy ΔH_m was determined from the total area of the peak between T_{onset}, when the DSC signal leaves the baseline, and T_{end}, when it reaches the baseline. ΔH_m was divided by the amount of fat and is then stated as the specific melting enthalpy Δh_m per unit mass of fat in J/g.

2.8. X-ray Diffraction Measurements

X-ray diffraction (XRD) measurements were performed by Annette Schucker at the Institute of Applied Materials and Electrochemical Technologies at the Karlsruhe Institute of Technology using an Empyrean X-ray diffractometer with a Bragg–Brentano geometry (Malvern Panalytical, Worcestershire, UK). The X-ray source was a copper tube operating at 60 kV and 100 mA. One sample droplet was pipetted onto a zero-diffraction plate and evenly distributed to obtain a plain surface. Diffraction patterns were acquired at 22 °C and at 2θ diffraction angles of −111–168° using a 15° rad/s scanning rate. The data were postprocessed using DiffracPlus, and PDF2 was used as the reference database. For the y-axis, the detection angle 2θ was translated into the distance between the set of parallel planes in the fat crystals, i.e., the d-spacing Å, according to Equation (2). Based

on the diffraction pattern of a crystalline sample and the wavelength λ of the incident X-rays, Bragg's law allows the translation of the peak position, i.e., the detection angles at which diffraction peaks are recorded, into the distance or *d*-spacing d_{hkl} (with the vector coordinates *hkl*) between the set of parallel planes that the peaks originate from [61]:

$$\lambda = 2d_{hkl}\sin\theta \quad (2)$$

2.9. Statistical Analysis

All samples were prepared two times independently. All measurements were performed at least three times, if not stated otherwise. Uncertainty was calculated using Origin 2022b (OriginLab Corporation, Northampton, MA, USA), and the result is expressed as standard error of the mean (SEM). The data were also checked for normal distribution using the Shapiro–Wilk test. Normally distributed data were analyzed using one-way analysis of variance (ANOVA) with a significance level of $p^* < 0.05$. For non-normally distributed data, the Kruskal–Wallis or Mann–Whitney test, which are non-parametric analytical methods to assess variance, was performed.

3. Results

3.1. Dispersion Characterization after Production

3.1.1. Particle Size Distribution

The volume-based particle size distributions ($Q_3(x)$) of dispersions directly after slow and fast cooling are depicted in Figure 1a,b, respectively. In general, the distributions of all samples are polydisperse: particles between 0.2 µm and 100 µm were measured. The sample *Ref slow* shows the broadest distribution with particles up to 100 µm. The sample *Chol 0.1 slow* also has a broader distribution compared to the rest of the slowly cooled samples. The narrowest distribution and smallest particles in dispersions are found in the sample *Chol 0.05* and the sample *Eta 0.05* after fast cooling. In general, the size distributions of the rapidly cooled dispersions are narrower and more monodisperse compared to the size distributions of the slowly cooled samples, and no particles larger than ~25 µm are found in the rapidly cooled samples. However, the measured differences are not very pronounced overall.

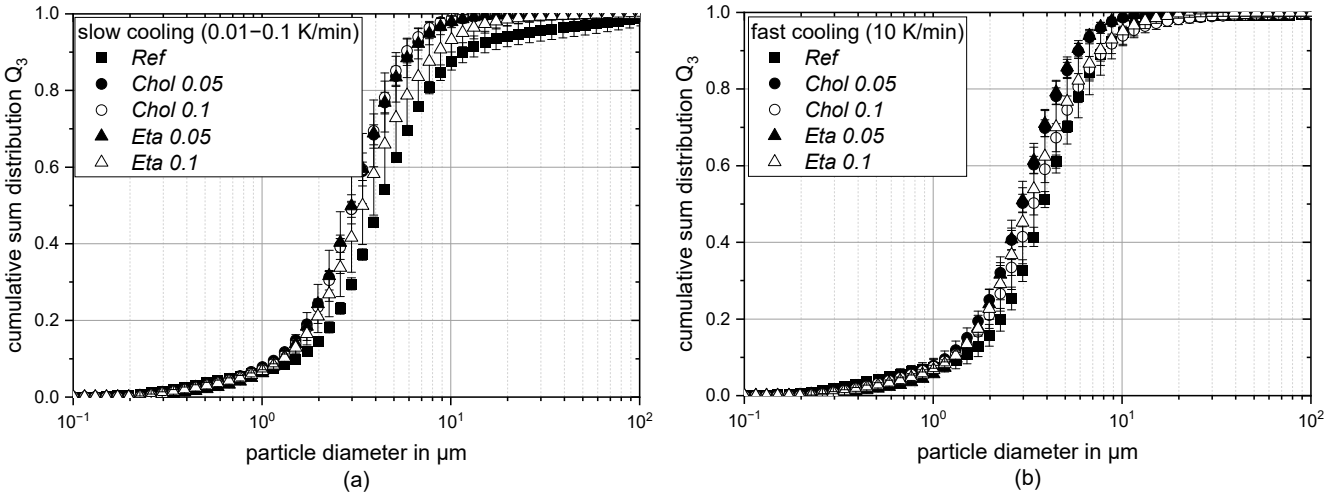

Figure 1. Cumulative volume sum distribution of dispersions stabilized with β-lg (*Ref*), β-lg + PC (*Chol*) and β-lg + PE (*Eta*) directly after cooling (t_0) at a slow (**a**) or fast cooling rate (**b**).

3.1.2. Particle Morphology and Dispersion Microstructure

The particle morphology and general microstructure of particles stabilized with the different emulsifier systems were assessed microscopically directly after production. Exemplary microscopic images obtained after slow cooling and fast cooling are depicted in

Figure 2. Spherical particles were obtained in all cases, and the ones visible in the sample aliquots appear as luminous green and yellow colors under the polarized light microscope, meaning they were fully crystalline after the applied cooling processes. However, submicron-sized particles are not visible under light microscopy. Thus, no conclusions about their crystallinity can be drawn.

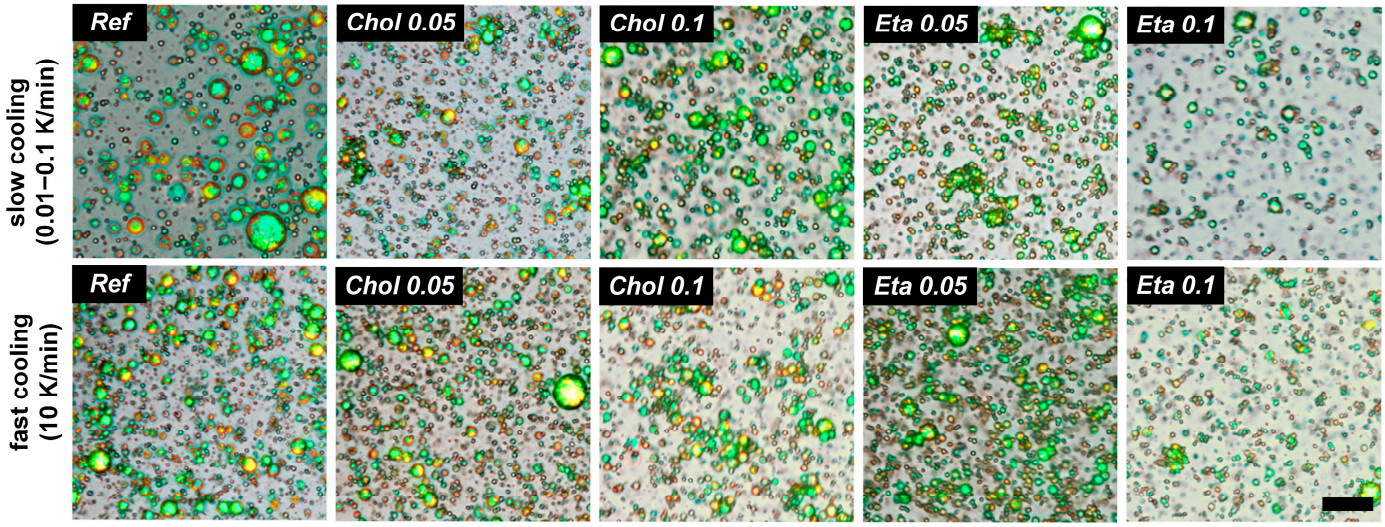

Figure 2. Exemplary microscopic images of undiluted dispersions stabilized with β-lg (*Ref*), β-lg + PC (*Chol*) and β-lg + PE (*Eta*) directly after cooling (t_0) at a slow and a fast cooling rate. PLs were used in concentrations of 0.05 wt% (*Chol 0.05* and *Eta 0.05*) and 0.1 wt% (*Chol 0.1* and *Eta 0.1*). The length of the scale bar is 25 μm.

Particle aggregation can be seen in the microscopic images of all samples. As the majority of these aggregates consist of two or more particles maintaining their individual integrity, we assume flocculation has taken place. Flocculation seems to be slightly more pronounced in the samples containing PLs, especially in the samples crystallized at a slow cooling rate. The *Eta* samples show the highest number of flocculated particles. The flocs involve more particles compared to the *Ref* and *Chol* samples and, therefore, reach a similar size even though the individual particles forming the flocs appear smaller.

3.1.3. Dispersion Viscosity and Flow Behavior

The dispersion viscosity as a function of the shear rate obtained for samples after slow cooling is depicted in Figure 3a, and after fast cooling in Figure 3b. In all samples, the viscosity decreases with increasing shear rate, which is typical shear thinning behavior for crystalline dispersions. The curves start to reach a plateau at low shear rates, characterizing a system with zero shear viscosity. Overall, the viscosities lie in the range of 3×10^1–2×10^2 mPa·s, with the highest value measured for the sample *Chol 0.1 fast* (cf. Figure 3b). The viscosity drops at low shear rates, i.e., below 1 s^{-1}, which is most pronounced in the curve of the sample "*Ref slow*", as shown in Figure 3a.

3.2. Storage Behavior of Dispersions

3.2.1. Macrostructure and Creaming Index

The macrostructure of the samples was assessed optically regarding their creaming behavior. The pictures were used to determine the creaming index (*CI*) of the samples, and the results can be found in Figures S1–S3. The total sample volume decreased over time as aliquots were taken to perform different analytical measurements.

An exemplary picture of a sample container is shown in Figure 4. All samples, irrespective of the formulation, cooling procedure or storage time, appear heterogeneous. A white opaque top layer is visually separated from the main serum layer. This is already

the case after the cooling procedure and before storage. The main serum layer is also split into a thin, clear layer at the bottom of the sample container and a large amount of the remaining phase. After slight shaking of the sample vessels, all samples are visually homogeneous again.

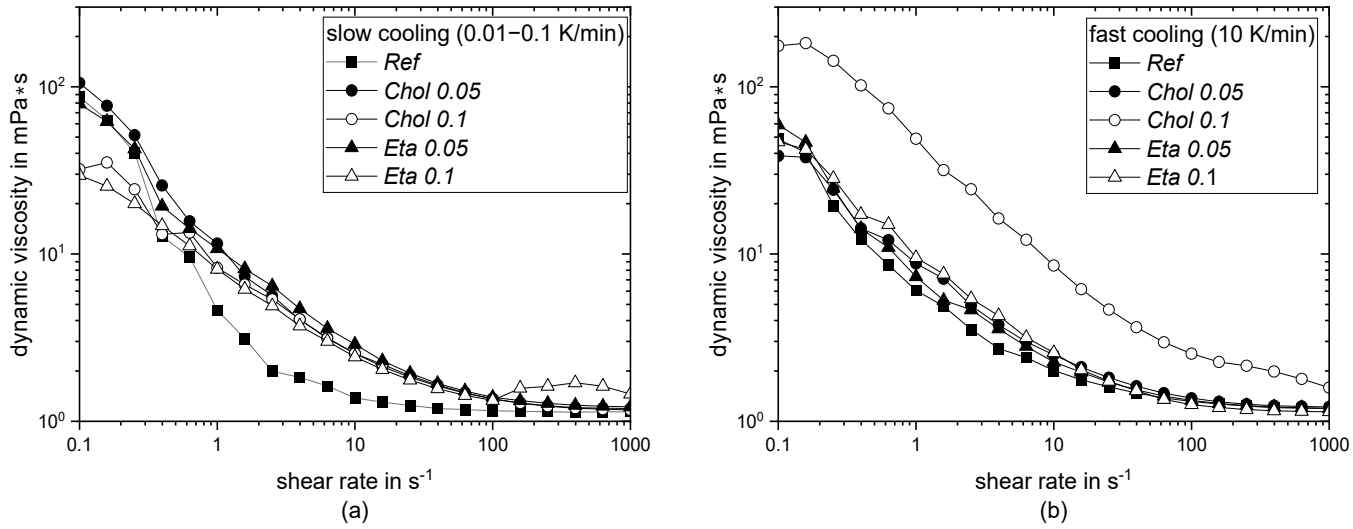

Figure 3. Viscosity (η) as a function of shear rate ($\dot{\gamma}$) of dispersions stabilized with β-lg (*Ref*), β-lg + PC (*Chol*) and β-lg + PE (*Eta*) directly after cooling (t_0) with a slow cooling rate (**a**) and a fast cooling rate (**b**). PLs were used in concentrations of 0.05 wt% (*Chol 0.05* and *Eta 0.05*) and 0.1 wt% (*Chol 0.1* and *Eta 0.1*). Measurements were performed at 22 °C.

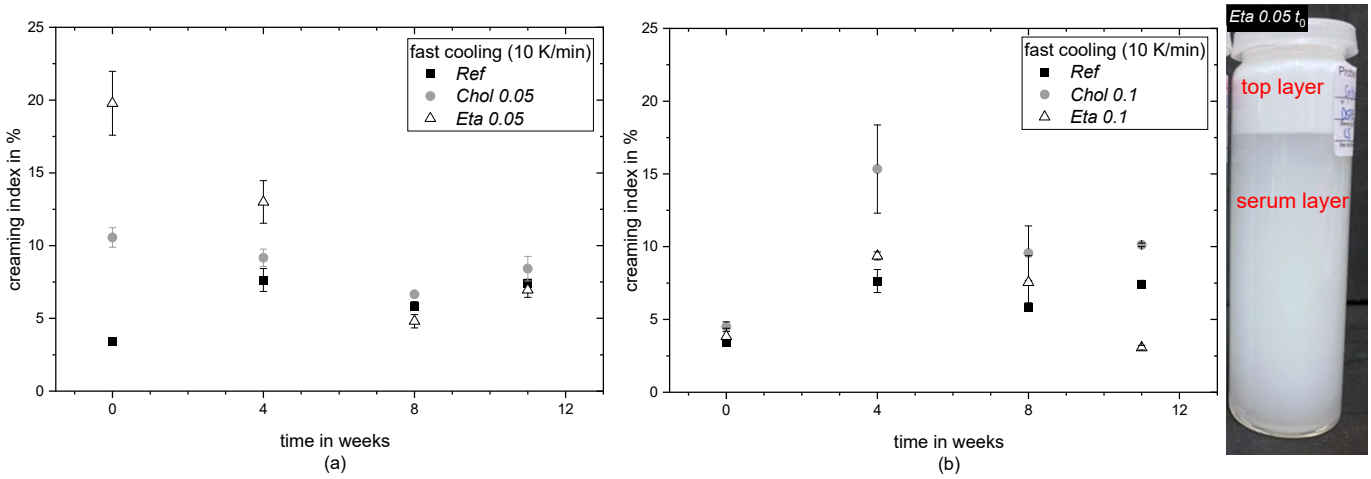

Figure 4. Creaming index (*CI*) of dispersions stabilized with β-lg (*Ref*), β-lg + PC (*Chol*) and β-lg + PE (*Eta*) as a function of storage time: directly after preparation (t_0), after four weeks (t_4), after eight weeks (t_8) and after eleven weeks (t_{11}) of storage. PLs were used in concentrations of 0.05 wt% (*Chol 0.05* and *Eta 0.05* (**a**)) and 0.1 wt% (*Chol 0.1* and *Eta 0.1* (**b**)). The data of the samples cooled at a fast cooling rate are shown. The exemplary image of one sample is shown.

The *CI* over time is shown for the rapidly cooled dispersions in Figure 4a,b for a PL concentration of 0.05 wt% and 0.1 wt%, respectively. The *CI* for the slowly cooled samples can be found in Figure S4. The *Ref* sample is plotted in both figures. The Shapiro–Wilk test shows that the data are not normally distributed ($p = 0.05$); hence, the Kruskal–Wallis test was performed. At the beginning, the *CI* of the samples containing 0.05 wt% PLs, i.e., samples *Chol 0.05* and *Eta 0.05*, is 10% and 15% significantly higher than the *CI* of the remaining samples. This means that the height of the top creamed layer in relation to the overall sample height is significantly larger in these two samples, and creaming has

occurred to a larger extent directly after preparation. Over the eleven weeks of storage, the *Ref* samples showed a constant increase in the *CI* from 3 5% to 7–11%. The creamed top layer grew larger in height and was more rigid over time in the *Ref* samples. To allow a homogeneous sampling process, the sample container was gently inverted three times; after this, the *Ref* samples stayed heterogeneous. The samples containing PLs, i.e., samples *Chol* and *Eta*, exhibited an opposite tendency, i.e., a decrease in *CI* from 10–15% to 5–7%. The absolute height of the top layer dropped after four weeks of storage and, in contrast to the *Ref* sample, the creamed top layer was not rigid and was always easily miscible upon gentle agitation. The Kruskal–Wallis test performed on the *CI* showed no statistically significant effects.

A difference in turbidity of the main serum phase between the *Ref* samples and PL-containing samples is noted. While the main serum phase of the *Ref* samples was opaque over the observed storage period, this main serum phase of the PL-containing samples was significantly less turbid at t_0 and turned more turbid after eight weeks of storage (cf. Figures S1–S3). Overall, the PL-containing samples grew more homogeneous over time.

3.2.2. Particle Size

The particle size as a function of storage time for different emulsifier combinations of the rapidly cooled samples is shown in Figure 5a,b for a PL concentration of 0.05 wt% and 0.1 wt%, respectively. The data for the slowly cooled samples can be found in Figure S5. The 90% (x_{90}) and 10% (x_{10}) percentiles of the Q_3 distribution are also shown.

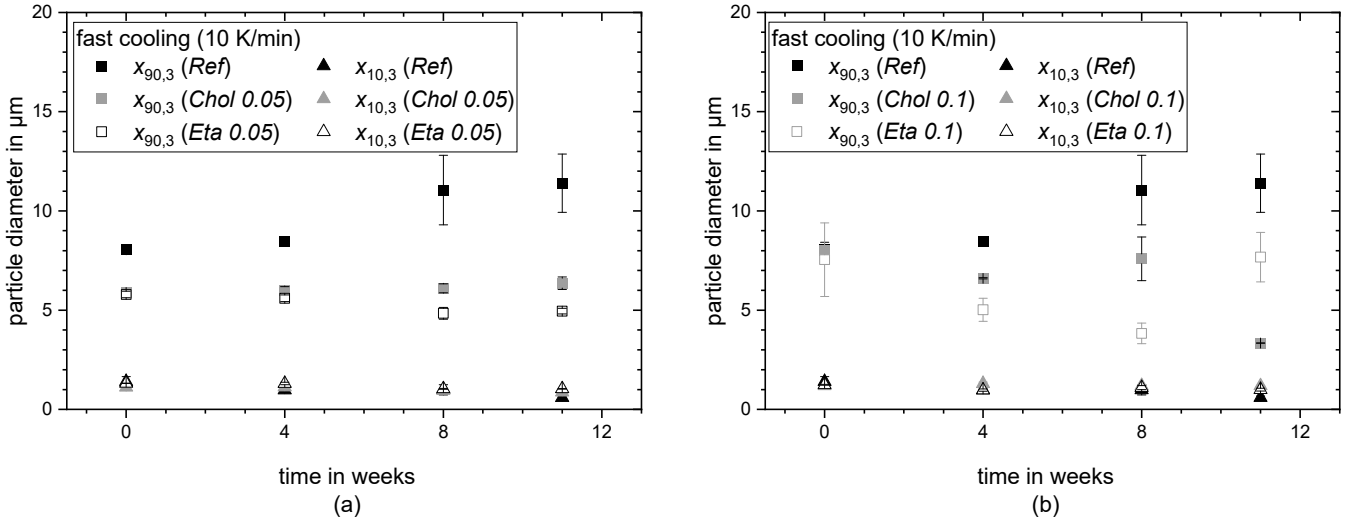

Figure 5. The 10% and 90% percentiles of the cumulative size distribution based on the particle volume. Data are shown for dispersions stabilized with β-lg (*Ref*), β-lg + PC (*Chol*) and β-lg + DSPE (*Eta*) as a function of storage time: directly after preparation (t_0), after four weeks (t_4), after eight weeks (t_8) and after eleven weeks (t_{11}) of storage. PLs were used in concentrations of 0.05 wt% (*Chol 0.05* and *Eta 0.05* (**a**)) and 0.1 wt% (*Chol 0.1* and *Eta 0.1* (**b**)). Data of the samples cooled at a fast cooling rate are shown.

The $x_{10,3}$ of the dispersion particles lies within a narrow range of 2–4 µm and remains constant over the storage period. The Shapiro–Wilk test shows that the data are normally distributed (p = 0.05). Therefore, one-way ANOVA (p = 0.05) was performed for the statistical significance, and the results can be found in Tables S1–S3. The initial $x_{90,3}$ differs significantly depending on the formulation; it is on average 30% higher in the *Ref* samples compared to the PL-containing samples. Over time, the $x_{90,3}$ changes significantly. The value of the *Ref fast* sample slightly increases in the first four weeks and then more extensively after eight weeks. The PL-containing samples show a completely different behavior. The *Chol 0.05 fast* sample and the *Eta 0.05 fast* sample show a more or less constant $x_{90,3,}$ with a small but not statistically significant decrease in the *Eta 0.05 fast*

sample after eight weeks. The *Chol 0.1 fast* and *Eta 0.1 fast* dispersions exhibit a significant decrease in $x_{90,3}$ over time. The $x_{90,3}$ of the *Eta 0.1 fast* sample constantly decreases and reaches a minimum value at t_8, which is on average 50% lower than at t_0. At t_{11}, the value significantly increases again. The *Chol 0.1 fast* sample first only shows a slight decrease in $x_{90,3}$ and then a significant drop at t_{11} to a value which is, on average, 50% lower compared to t_0. The significance in the change in $x_{90,3}$ was statistically confirmed, and the corresponding data and results of the one-way ANOVA can be found in Tables S1–S3 of the Supplementary Materials.

3.2.3. Melting Behavior

The melting thermograms obtained using DSC are shown in Figure 6 as the averaged curves for different formulations and cooling processes over storage time. The *y*-axis is omitted as the data were normalized to allow the representation of three measurement intervals in one diagram. Figure 6a shows the thermograms of the *Ref* samples, and Figure 6b,c depict the curves of the *Chol 0.05 slow* and *fast* samples and the *Eta 0.05 slow* and *fast* samples, respectively. In Figure 6d, one exemplary melting thermogram with the baseline is shown, and the occurring peaks are numbered to accentuate the endo- and exothermic events. In general, the melting curves comprise two endothermic events (melting peaks), i.e., a first melting endotherm around 47–48 °C (peak 1) and a second one at about 56 °C (peak 2), and one exothermic event (crystallization peak) with a peak temperature of 49–50 °C (peak 3), irrespective of the cooling rate and formulation. After eight weeks of storage, a third endothermic peak appears at a temperature varying between 41.5 °C and 44.9 °C, which is most visible in the *Eta 0.05 slow* sample and the *Chol 0.05 slow* sample. After eleven weeks of storage, this peak is not visible anymore. More detailed information about the samples' endo- and exothermic peak temperatures events can be found in Table S4–S8.

The endothermic peaks of the *Eta 0.05* samples are generally lower and flatter compared to the *Chol 0.05* samples and the *Ref* samples. The peak height decreases further in the *Eta 0.1* thermograms (cf. Figure S6).

The specific melting enthalpy Δh_m per unit mass of fat was determined using the corresponding melting peaks, and the result is summarized in Table 2. The Shapiro–Wilk test shows that the data are not normally distributed. The melting enthalpy per unit mass of fat of the *Chol 0.05 slow* and *fast* samples and the *Chol 0.1 slow* and *fast* samples is similar to that of the *Ref* samples, especially at the measurement intervals t_8 and t_{11}. The *Eta 0.05 slow* and *fast* samples have lower melting enthalpy values. This effect is even more pronounced for the *Eta 0.1 slow* and *fast* samples, with a decrease of approximately 50 % of the total melting enthalpy per unit mass of fat compared to the corresponding *Ref* samples. The lower melting enthalpy of the *Eta 0.1* samples compared to the *Ref* and *Chol* samples is statistically significant, which was accounted for by performing the Mann–Whitney test ($p = 0.05$). During storage, the melting enthalpy of all samples decreases at t_8 and then increases again at t_{11}, except for the *Eta 0.1 slow* and *fast* samples. Here, the melting enthalpy does not increase again. The Mann–Whitney test shows that the change in melting enthalpy over the storage time is not statistically significant ($p = 0.005$).

3.2.4. Polymorphism

The X-ray diffraction patterns for the different formulations and cooling procedures over the storage time are shown in Figure 7. Due to resource restrictions, the samples with 0.1 wt% PLs had to be excluded from the analysis, and only one measurement per sample was performed. The *y*-axis of the diagrams is omitted as the analysis was performed exclusively qualitatively to identify the peak positions and assign them to their respective polymorphs. The data sets were normalized to fit three curves into one diagram, corresponding to the three time intervals.

Table 2. Specific melting enthalpy per unit mass of fat for different formulations and cooling rates after preparation (t_0), after eight weeks (t_8) and after eleven weeks (t_{11}) of storage. The values are given as mean ± SEM (N = 2, n = 1).

	Specific Melting Enthalpy per Unit Mass of Fat, Δh_m, in J/g		
	t_0	t_8	t_{11}
Ref slow (0.01–0.1 K/min)	216.6 ± 74.7	128.3 ± 9.5	129.9 ± 9.3
Ref fast (10 K/min)	204.6± 42.6	124.2 ± 3.0	131.5 ± 0.5
Chol 0.05 slow (0.01–0.1 K/min)	137.5 ± 1.2	134.4 ± 1.6	144.9 ± 5.7
Chol 0.05 fast (10 K/min)	135.5 ± 12.0	122.6 ± 2.5	148.5 ± 3.7
Chol 0.1 slow (0.01–0.1 K/min)	146.0 ± 9.0	134.5 ± 18.7	146.8 ± 10.1
Chol 0.1 fast (10 K/min)	139.5 ± 8.6	144.2 ± 6.6	135.9 ± 25.8
Eta 0.05 slow (0.01–0.1 K/min)	92.9 ± 9.9	68.4 ± 12.1	100.3 ± 20.3
Eta 0.05 fast (10 K/min)	155.0 ± 47.6	112.4 ± 17.5	130.6 ± 12.4
Eta 0.1 slow (0.01–0.1 K/min)	52.2 ± 16.7	39.5 ± 9.0	33.2 ± 0.1
Eta 0.1 fast (10 K/min)	54.1 ± 14.2	67.7 ± 24.6	39.0 ± 16.5

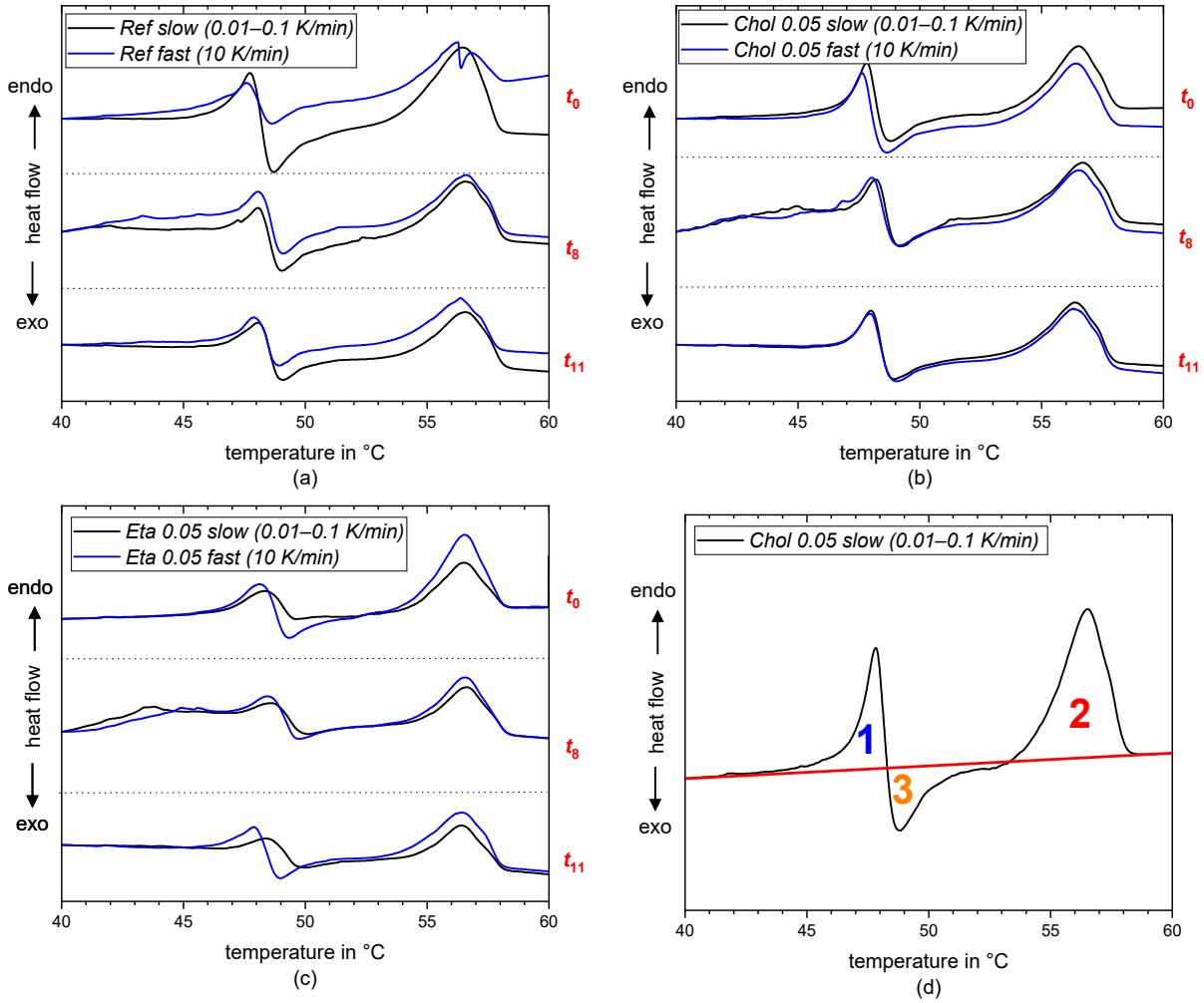

Figure 6. DSC melting thermograms of dispersions stabilized with β-lg (*Ref* (**a**)), β-lg + PC (*Chol 0.05* (**b**)) and β-lg + PE (*Eta 0.05* (**c**)) after slow (black lines) and fast (blue lines) crystallization directly after preparation (t_0), after eight weeks (t_8) and after eleven weeks (t_{11}) of storage. PLs were used in a concentration of 0.05 wt%. The curves have been displaced along the ordinate for better visualization. In graph (**d**), one thermogram is plotted to exemplarily show the baseline and highlight the endothermic and exothermic events: the two endothermic events are emphasized as peak 1 and peak 2, and the exothermic event is labeled as peak 3.

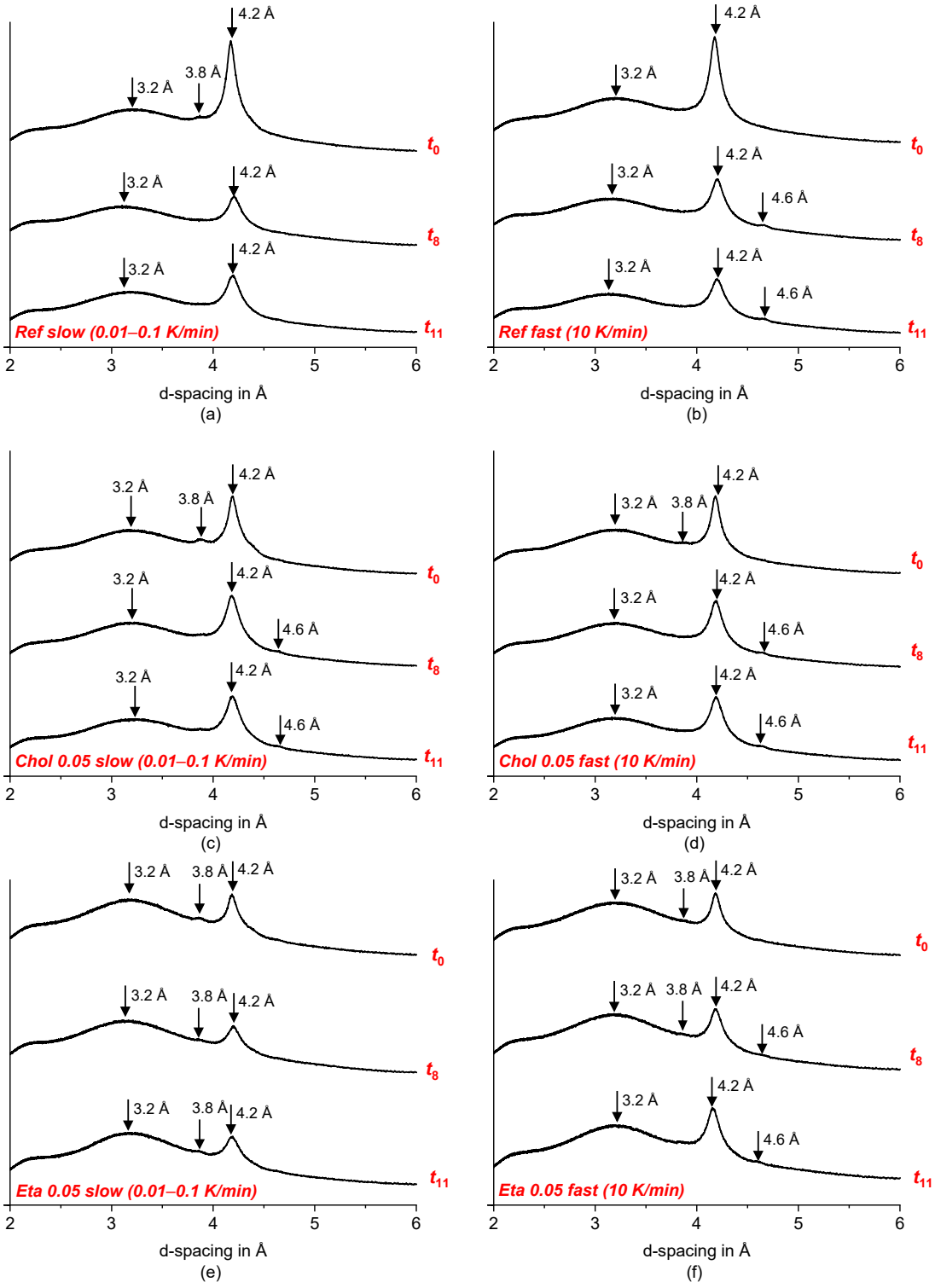

Figure 7. X-ray diffraction patterns of dispersions stabilized with β-lg (*Ref* (**a**,**b**)), β-lg + PC (*Chol 0.05* (**c**,**d**)) and β-lg + PE (*Eta 0.05* (**e**,**f**)) after slow and fast crystallization. PLs were used in a concentration of 0.05 wt%. Measurements were performed directly after preparation (t_0), after eight weeks (t_8) and after eleven weeks (t_{11}) of storage. The arrows point to detectable peaks.

All samples, irrespective of the cooling process, formulation and storage time, show a broad, flat peak at 3.2 Å, which does not match any reference values for the crystallographic data of TAG crystals. In all diffraction patterns, a prominent, narrow peak at 4.2 Å is found, and a very small peak at 3.8 Å, except for the *Ref fast* sample (cf. Figure 7b), can be identified

at t_0. These two peaks can be clearly assigned to the β′ polymorph of TAG crystals [48,62]. The height of the peak at 3.8 Å decreases over the storage time and disappears in all samples after eight or eleven weeks, except for the *Eta 0.05 slow* sample, where it is still slightly present after eleven weeks of storage. The presence of the α polymorph of TAGs can usually be detected using XRD, showing a broad peak with a d-spacing of 4.15 Å [62,63]. This peak is not present in any of our XRD patterns. However, the very distinct peak at 4.2 Å might overlap with the peak at 4.15 Å, and it might be difficult to separate these peaks. Therefore, we cannot exclude that α polymorph is present. After eight weeks, an additional peak at 4.6 Å is observed in the samples crystallized at a fast cooling rate and in the *Chol 0.05 slow*, which is characteristic for β polymorph [63].

4. Discussion

4.1. Influence of Phospholipid Addition and Cooling Procedure on Morphology, Particle Size and Visosity before Storage

Before comparing the colloidal stability of the dispersions during storage, the overall appearance and microstructure of the dispersions directly after preparation are discussed. All samples, irrespective of their formulation or cooling procedure, crystallized into spherical shape. This means no spontaneous self-shaping to polygonal platelets occurred during cooling, a process that has been reported for several TAG–surfactant combinations and cooling rates [64,65]. To induce self-shaping, the formation of a crystalline surfactant monolayer is necessary at a temperature above the oil bulk melting temperature. To date, it has not been shown that β-lg can crystallize at the droplet interface in this manner; thus, we did not expect any self-shaping in the *Ref* samples. As we only observed spherical particles in the *Chol* and *Eta* samples as well, we assume that the chosen PLs were also not able to crystallize at a temperature relevant for self-shaping and, therefore, did not provide the necessary crystalline monolayer.

The addition of PLs (*Chol* and *Eta*) led to differences in particle size and flocculation behavior compared to dispersions stabilized with β-lg alone (*Ref*). As expected, the particles in the *Ref* samples were bigger compared to the ones in the *Chol* and *Eta* samples. The largest particles and most polydisperse distribution were measured in the *Ref* slow dispersions, whereas smaller particles and narrower distributions were obtained with PL addition and fast cooling. The assumption that the addition of PLs as emulsifiers would result in smaller particle sizes is confirmed by our results. However, flocculation was more pronounced in the PL-containing samples and occurred most extensively in the *Eta 0.1* samples. We assume that the particles are stabilized by a mixed interfacial layer consisting of β-lg and PLs. A total displacement of proteins by PLs is not expected as the emulsifiers are known to be able to coexist at the oil–water interfaces [27]. LMWEs and proteins have been shown to undergo complexation when co-adsorbed at the particle surface, where they may undergo structural changes and result in new characteristics compared to those of the individual emulsifiers [20,28,29]. However, with the data available to us here, we cannot decide whether complexation has occurred and whether this is responsible for the increased tendency toward flocculation.

In addition to the emulsifier used, the cooling procedure had an influence on particle size. As expected, slow cooling resulted in larger particles and broader size distributions compared to fast cooling. During slow temperature changes, droplets remain liquid for a longer time as the necessary supercooling is reached later. This gives the droplets more time to partially and fully coalesce before their liquid–solid phase transition, resulting in larger particles [66].

The dispersions all show shear thinning behavior irrespective of the emulsifier combination or cooling procedure, which is often found for crystalline dispersions. In the slowly cooled samples, the zero shear viscosity was lower when high concentrations of PL were present, but the drop in viscosity with increasing shear rate was most pronounced in the *Ref* samples. As the *Ref slow* sample also had the broadest size distribution and largest particles, this could be the reason for the differences in flow behavior. The dispersions

cooled at a fast rate showed very similar viscosities, except for the *Chol 0.1* sample, which had a significantly higher viscosity. This corresponds with a dispersion of medium-chain TAGs stabilized with WPI/Tween® 80 in the presence of the PL phosphatidylserine. Here, the viscosity increased with decreasing droplet size [60]. The authors related this to more hydrodynamic interaction. As increasing concentration of LMWEs resulted in smaller droplet sizes in their system, they argued for this to account for the increase in viscosity with increasing emulsifier concentration. As we observed the highest viscosity with the highest PL concentration, increased interactions might have accounted for the increase in viscosity and small particle sizes, even when the particle size was not significantly smaller compared to the other samples. In addition, the cooling rate seems to have a clear effect on the aggregation processes of the *Chol 0.1* samples, which might account for the higher viscosity in this case. This behavior and the possible reasons behind it could be studied in-depth in future work.

4.2. Influence of Phospholipid Addition and Cooling Procedure on Dispersion Stability during Storage

4.2.1. Assessment of Creaming Behavior and Changes in Micro- and Macrostructure Depending on Phospholipid Addition and Cooling Procedure

The observed phase separation in all samples is the result of creaming of the dispersed phase. Creaming in short periods of time is expected, as all dispersions depict particles well above 1 µm, and TAG particles float due to their lower density. Flocculation and/or (partially) coalescence during storage increases particle size and, thus, creaming velocity [67]. In consequence, the concentration of fat particles decreases all the way to the bottom of the sample container. Therefore, the lower phase appears brighter. The thin, very clear bottom phase is probably completely void of fat particles or contains only fat particles below the optically detectable size of about 100 nm. As the phases in the PL-containing dispersions were miscible again upon agitation, the fat particles in the creamed layer were probably flocculated and not coalesced, which is in good agreement with the microscopic images. The creamed layer in the *Ref* samples appeared more rigid and was not as easily miscible, which is a strong indication for non-reversible aggregation and/or coalescence. This aggregation might have also been provoked by bridging between the protein-covered particles' surfaces. As no rigid creamed layer was observed in the *Eta* and *Chol* samples and the phases were easily miscible again, the PL addition seemed to have prevented the non-reversible aggregation induced by proteins. In addition, we observed a decreasing creaming index in the samples containing PLs over time, meaning that the dispersions were more homogeneous. These results strongly indicate that the addition of PLs increases the colloidal stability of the dispersions as expected. The co-adsorbed emulsifier could have had a beneficial effect on the elasticity of the creamed layer and the general colloidal stability over the storage period.

The decreasing *CI* over time was most pronounced for the *Eta 0.1* samples, irrespective of the cooling rate. This was contrary to our expectations as we assumed a higher colloidal stability in the Chol samples due to the larger hydrophilic head group. We also observed that the serum phase of the *Ref* emulsions with β-lg alone were highly opaque and white over the total storage period, whereas the PL-containing samples had a clear serum phase at the beginning which turned turbid and white after eight weeks of storage. In addition, the flocs that were present in the PL samples directly after preparation became less over the observed storage period. We assume that during storage, the displacement of β-lg by PLs took place, resulting in the dissolution of flocs. This would be consistent with the findings reported by McClements et al. [68], who showed that the addition of LMWE leads to the dissolution of flocs via the displacement of proteins from the interface.

However, our experimental design was based on analytical methods, which do not allow us to draw conclusions on the actual composition of the interfacial layer and its changes over time. We characterized macro- and microstructural changes and gained information about the global characteristics of the dispersions, but the physical chemistry and underlying molecular structures and their changes were not part of our study. Thus,

future work should include analytical methods that could elucidate molecular interfacial phenomena to gain a deeper understanding of the underlying mechanism.

With regard to the cooling procedure, the expected enhanced colloidal stability for the samples cooled at a fast cooling rate, compared to the samples cooled at a slow cooling rate, was not observed. Even though we obtained smaller particle sizes and narrower distributions with fast cooling, the colloidal stability was not significantly improved by this. No clear trend could be derived from the change in *CI* and dispersion microstructure over time when comparing the cooling rates. It appears that the formulation has a greater impact than the cooling rate on these phenomena for the investigated model systems.

4.2.2. Assessment of Changes in Particle Size Macrostructure Depending on Phospholipid Addition and Cooling Procedure

There are several colloidal instability mechanisms that can lead to changes in the average particle diameter and size distribution, i.e., flocculation, (partial) coalescence or Ostwald ripening. Even though we found no correlation between the applied cooling rate and colloidal instability, the PL addition had a pronounced impact on colloidal instability mechanisms, leading to changes in particle size compared to the use of β-lg alone.

Over the course of sample storage, the median and $x_{10,3}$ of all samples remained nearly constant, deviating only by ±1 µm. However, the $x_{90,3}$ of all *Ref* samples increased over the storage time. Changes in the lower particle size range are not expected to have a significant impact on the colloidal stability of dispersions, but bigger particles are expected to have an impact. Flocculation, aggregation and (partial) coalescence will be easily detected by changes in $x_{90,3}$ since volume increases with the third power of size. Ostwald ripening with lager particles growing at the expense of smaller ones will mostly result in changes in the $x_{90,3}$ and $x_{10,0}$ values, but the latter were not evaluated here. The $x_{90,3}$ showed a clear time- and formulation-dependent tendency. It increased significantly in the *Ref* samples over the observed storage period, which is in good accordance with the rigid creamed top layer, is typical for (partly) crystalline dispersions, and is consistent with the instability mechanisms reported in the literature [8,9,14,69].

The samples containing PLs did not exhibit an increase but rather a decrease in $x_{90,3}$, (cf. Figure 5), which was not expected. This effect was more pronounced with 0.1 wt% PL compared to 0.05 wt% PL. In general, the particle size measurements results are in good agreement with the observations of the macrostructure, where the *Chol* and *Eta* dispersions visually became more homogeneous over time (cf. Figures S1–S3). The decreasing particle size and the increasing homogeneity are rather uncommon with regard to colloidal instability mechanisms in O/W emulsions and dispersions. On the one hand, the decrease in particle size and increase in sample homogeneity could be interpreted as increased colloidal stability compared to the samples stabilized by β-lg alone. On the other hand, the particle decrease indicates that mass transport processes have occurred between fat particles. These processes would lead to a redistribution of TAG molecules between the particles and could, therefore, entail a change in the particle size distribution in the observed manner. If an emulsified fat acts as a carrier for drugs, functional ingredients or additives, the diffusion of TAG molecules can affect the delivery, stability and functionality of these hydrophobic agents, or even release them during storage. It has been shown that compositional ripening and solubilization can occur in TAG emulsions [68,70]. McClements et al. [68] argued that these two processes generally dominate over Ostwald ripening as a difference in Laplace pressure is lower than the driving force for compositional ripening and solubilization, i.e., the entropy of mixing. They assumed this contributes to the fact why they did not see an increase in droplet size, which might also lead to the changes we observed in our samples. Samtlebe et al. [70] reported the migration of individual fat molecules between a fraction of liquid emulsion droplets and a fraction of solid lipid nanoparticles (SLNs). They proposed that liquid oil gets solubilized in the aqueous phase, diffuses to the surface of SLNs, adsorbs at their surface and dissolves solid fat crystals in the adsorbed surface layer. The dissolved fat crystals would then diffuse in the opposite direction, i.e., toward

liquid oil droplets, which would further enhance the entropically favorable mixing process. It is reasonable that our systems also contain fully solidified TAG particles, as well as partially crystalline and supercooled liquid TAG droplets. This can be attributed to the different FAs present in the dispersed phase, as well as the fact that emulsified fats show a crystallization behavior different from that of bulk fats. The crystallization of dispersed droplets is a stochastic and individual process, which differs from droplet to droplet and occurs over a wide temperature range [30,32]. A significantly higher level of supercooling is needed, which even increases with decreasing droplet size [33,34]. Thus, we assume that there is an overall unequal distribution of both high-melting and low-melting and solid, semi-crystalline and liquid TAG fractions over the particles. This would enhance the mass transport processes between the particles until reaching an equilibrium distribution of different TAG molecules.

Mass transport processes can also be expected to be enhanced in the presence of β-lg. This protein has a very specific tertiary structure which allows binding and transport of polar ligands. Excess β-lg might, therefore, be able to bind individual, liquid TAG molecules to the hydrophobic pocket, thereby enhancing inter-droplet mass transfer processes. As LMWEs are also known to displace proteins from particle interfaces, this might explain why the decrease in $x_{90,3}$ occurred in the PL-containing samples over time. The displaced β-lg gets solubilized in the continuous phase and is available for binding of apolar ligands. This is further supported by the observation that the serum phase of the samples differed in its turbidity depending on the emulsion formulation. While the serum phase of the *Ref* dispersions was highly opaque and intensely white over the total storage period, the phospholipid-containing samples had a clear serum phase that turned turbid and white only after eight weeks of storage. As these differences cannot be related to the size difference, we hypothesize that the opacity of the serum phase is connected to the amount of solubilized protein and complex formation with the presence of PLs. Consequently, we hypothesize that proteins did desorb from the particle surface in the PL-containing samples over the storage time, and the soluble protein fraction in the serum phase increased and met the level of the *Ref* samples. This hypothesis is supported by the proposed mechanism that the addition of small amounts of PLs can increase the interfacial load of ß-lg [27], which may explain the differing turbidity at t_0. However, as we only observed the change in turbidity after several weeks of storage and did not expect this to happen, we did not quantify the amount of β-lg in the serum phase and the concentration changes. Future studies should, therefore, further look into the interfacial load of β-lg and the potential changes of β-lg concentration in the serum phase using, for example, the Bradford or BCA method.

In addition to a decrease in particle size, an increase in $x_{90,3}$ of the *Eta 0.1 fast* sample was observed between week 8 and week 11. Hence, colloidal instabilities, such as (partial) coalescence, aggregation and Ostwald ripening, must have now prevailed over the changes in particle size due to the mass transport phenomena. This could be interpreted as a worsening in the colloidal stability of the *Eta* samples compared to the *Chol* samples. However, we expected a much more pronounced effect. Our results do not support our hypothesis of improved colloidal stability with a more hydrophilic PL being present.

4.2.3. Assessment of Polymorphic Transitions and Dispersion Crystallinity Depending on Phospholipid Addition and Cooling Procedure

Besides colloidal stability, we found evidence for polymorphic transitions over the storage time. Polymorphic transitions are known to promote flocculation because the rearrangement of one crystal form into another exposes patches on the particle surface that are not covered by emulsifier molecules [69,71].

Based on the results described in Section 3.2.3, it can be concluded that the dispersed TAG particles existed in β′ polymorph in all samples independent of the formulation or cooling process. The samples crystallized at fast cooling rates and all Chol samples showed evidence of polymorphic transitions from β′ to β polymorph. We did not detect

the presence of α polymorph in any of our samples using XRD. As polymorphic transitions are assumed to enhance aggregation, fast cooling and *Chol 0.05* should have shown an increase in particle size, which would have been contrary to our assumptions. However, the influence of these polymorphic transitions on the colloidal stability of our model systems must be minor, as no extensive aggregation was observed for these samples, and they did not exhibit significant increases in particle size. The remaining β-lg and PLs in the serum phase were most likely able to cover the particle surfaces newly revealed by the polymorphic transition.

The XRD patterns also help to interpret the observations made on the melting behavior of the samples. The DSC patterns are marked by two distinct endothermic events and one exothermic event, which is highly uncommon in emulsified fats. They usually result in flat and very broad peaks, which often merge into each other [33]. The exotherm peak has a peak temperature between 47 °C and 49 °C and appears right after the first endothermic peak (cf. Figure 6). Thus, a crystallization event must have taken place during heating, which is most likely the result of a polymorphic transition. A polymorph with a low melting temperature melts and then crystallizes into a polymorphic form with a higher melting temperature. This polymorph then melts again upon further heating, resulting in a second endothermic peak at approximately 56 °C. In the literature, melting temperatures of 45 °C and 56 °C for α and β′ polymorphs, respectively, have been reported for tripalmitin [22,72]. We, therefore, assume that the first endothermic event in our DSC patterns indicates the melting of α polymorph, which recrystallizes as β′, resulting in the exothermic event. The second endothermic event at 56 °C may then be attributed to the melting of the old and newly formed β′ polymorphic forms. Melting of β crystals should then occur at higher temperatures at around 66 °C. We did not observe any endothermic events at this temperature. The peaks in the XRD patterns which can be attributed to β polymorph are small compared to the peaks accounting for β′ polymorph, which is why we assume that the amount of β crystals is too low to be detectable in the DSC measurements.

The DSC and XRD patterns reveal another relevant piece of information. The DSC peak area and height and the XRD peak height of the Eta samples are significantly lower compared to the rest of the samples. This effect seems to be concentration dependent as the peak area is reduced by 30% and 50% in the *Eta 0.05* and Eta 0.1 samples, respectively, when compared to the *Ref* samples. Due to resource restrictions, the samples with higher PL concentration were excluded from the XRD analysis. However, it is reasonable to assume the same tendency would have been corroborated. As the area integrated over the endothermic peaks serves to qualitatively compare the amount of crystalline matter in the sample aliquots, this result suggests that PE has an inhibitory effect on TAG crystallization. Hence, a higher crystallinity was achieved in the Chol samples compared to the *Eta* samples. We expected this is due to the larger hydrophilic headgroup of PC compared to PE and, therefore, its greater interfacial affinity inducing surface heterogeneous nucleation. However, we did not expect a lower crystallinity in the *Eta* samples compared to the *Ref* samples. This means PE must have somehow inhibited droplet crystallization, which should be investigated in future studies. The lower crystallinity of the *Eta* samples compared to the *Chol* samples might be the explanation for why the decrease in the $x_{90,3}$ was most pronounced in the *Eta 0.1 fast* sample in the first eight weeks of storage. As both liquid oil and solid fat are needed for the mass transport phenomena, which we assume took place, it is logical that they occurred faster when more liquid oil was present. In addition, these mass transport phenomena seemed to be finished after eight weeks in the *Eta 0.1 fast* samples as an increase in $x_{90,3}$ was observed between week 8 and week 11. We assume that the decrease in particle size due to the mass transport phenomena was then superimposed by (partial) coalescence, flocculation and irreversible agglomeration. In the *Chol 0.1 fast* samples, the $x_{90,3}$ dropped most extensively between week 8 and week 11, meaning that the mass transport process took place slower. It is reasonable to assume that the higher crystallinity in the *Chol* samples slowed down the mass transport process. On the one hand, this retarded transport could be interpreted as increased colloidal stability when a more hydrophilic PL is present. On

the other hand, for certain applications, it might be advantageous to suppress the TAG mass transport fully.

5. Conclusions

In this study, the addition of PLs to β-lg-based emulsions was investigated as a factor that could potentially lead to smaller crystal size, a higher crystallinity, delayed polymorphic transitions and reduced colloidal instabilities, compared to using β-lg alone. Furthermore, we expected a greater effect when using a PL with a larger hydrophilic headgroup and, thus, a greater interfacial affinity compared to a more hydrophobic PL.

The observations made on the macro- and microstructure of the dispersions and the results of the laser diffraction analysis provide reasons to assume that the PLs were successfully adsorbed to the particle interface and interacted with the proteins at the interface. The PL-containing samples appeared more homogeneous compared to the *Ref* samples, in which a rigid creamed layer developed quickly over time. In contrast to the PL-containing samples, this creamed layer could not be dispersed evenly by mixing. In this regard, the co-adsorbed PLs would have a beneficial effect on the general colloidal stability over the storage time. Considering the particle size distributions, unexpected changes over time were observed. The 90% percentile representing big flocs or coalesced particles increased over time in the *Ref* samples, which is in good accordance with the aggregation observed under the microscope and the increased rigidity of the creamed layer. In contrast, a decrease in $x_{90,3}$ was generally observed in the PL-containing samples, indicating a reduced tendency toward flocculation and aggregation.

However, we did not observe the expected influence of the hydrophilic headgroup on colloidal stability. In our study, the model systems with the addition of PL concentration of 0.05 wt% appeared very homogeneous after eleven weeks of storage. They exhibited practically no changes in particle size, irrespective of PL hydrophilicity. Hence, the addition of the right amount of PLs may increase the colloidal stability of a β-lg-based dispersion.

The DSC measurements did not reveal higher crystallinity in the samples containing PLs compared to the Ref samples. PC had no influence on the solid fat content (SFC) and PE seemed to even inhibit fat crystallization. The DSC patterns of the dispersions also helped to interpret the observations made using XRD as we observed very clear and distinct melting and crystallization peaks, which are typically known for polymorphic transitions in bulk fat systems. We were not able to correlate the observed polymorphic transitions with increased colloidal stability. We assume that the excess amounts of β-lg and PLs present in the serum phase were able to cover the free patches on the particle interface exposed by the polymorphic conditions.

In addition to formulation, we investigated the influence of cooling rate, i.e., fast and slow cooling, on the colloidal stability of the model systems. Fast cooling did result in a narrower and more monodisperse particle size distribution. However, we found no clear evidence of delayed polymorphic transitions. The colloidal instability mechanisms we observed during the storage of the dispersions were also not significantly improved by a fast cooling rate (10 K/min), or even faster cooling rates would have been needed. As a fast cooling process is highly energy demanding and does not bring a clear benefit for the colloidal stability of the model systems, it would be neither cost efficient nor sustainable to apply a high cooling rate to crystallize dispersed TAGs stabilized by β-lg alone or in combination with PLs.

Importantly, we acknowledge some limitations in this study. Our experimental design was focused on phenomena associated with colloidal stability. Therefore, it excluded analytical methods that would have allowed us to draw conclusions about the actual molecular composition of the interfacial layer and its changes over time. Future research should attempt to gain a deeper understanding of the underlying mechanisms and try to localize PLs and analyze their interaction with β-lg at the droplet interfaces.

To conclude, our study revealed some unexpected storage behavior of whey proteins and phospholipid-containing (semi-)crystalline dispersions. The addition of PLs had both beneficial and adverse effects on colloidal stability during storage. Depending on the application, the use of PLs in protein-based systems might be beneficial for colloidal stability, but mass transport phenomena must be closely monitored.

Supplementary Materials: The following supporting information can be downloaded at: https://www.mdpi.com/article/10.3390/colloids7020045/s1, Figure S1: Images of the *Ref* samples, Figure S2: Images of the *Chol 0.05* and *Chol 0.1* samples, Figure S3: Images of the *Eta 0.05* and *Eta 0.1* samples, Figure S4: Creaming index (*CI*) of samples cooled at a slow cooling rate, Figure S5: The 10% and 90% percentiles of the cumulative size distribution based on the particle volume of samples cooled at a slow cooling rate, Figure S6: DSC melting thermograms of dispersions stabilized with 0.1 wt% PL, Table S1: The 90% percentile of the cumulative normalized undersize distribution of the *Ref* samples., Table S2: The 90% percentile of the cumulative normalized undersize distribution of the *Chol 0.05* and *Chol 0.1* samples., Table S1: The 90% percentile of the cumulative normalized undersize distribution of the *Eta 0.05* and *Eta 0.1* samples. Table S2: Peak melting and crystallization temperature of the endo- and exothermic peaks in the DSC curves of the *Ref* samples, Table S5: Peak melting and crystallization temperature of the endo- and exothermic peaks in the DSC curves of the *Chol 0.05* samples, Table S6: Peak melting and crystallization temperature of the endo- and exothermic peaks in the DSC curves of the *Chol 0.1* samples, Table S7: Peak melting and crystallization temperature of the endo- and exothermic peaks in the DSC curves of the *Eta 0.05* samples, Table S8: Peak melting and crystallization temperature of the endo- and exothermic peaks in the DSC curves of the *Eta 0.1* samples.

Author Contributions: Conceptualization, J.R.; methodology, J.R.; formal analysis, C.S.; investigation, C.S. and J.R.; resources, H.P.K.; data curation, C.S. and J.R.; writing—original draft preparation, J.R.; writing—review and editing, V.G. and H.P.K.; visualization, C.S. and J.R.; supervision, V.G. and H.P.K.; funding acquisition, H.P.K. All authors have read and agreed to the published version of the manuscript.

Funding: This research was conducted in the framework of the IGF Project no. 21099 N of the FEI and was supported via the AiF within the program for promoting Industrial Collective Research (IGF) of the German Ministry of Economic Affairs and Energy (BMWi), based on a resolution of the German Parliament.

Data Availability Statement: The datasets generated for this study are available from the corresponding author upon request.

Acknowledgments: We acknowledge support provided by the KIT-Publication Fund of the Karlsruhe Institute of Technology. The authors also thank IOI Oleo GmbH (Hamburg, Germany) for providing Softisan® 154 and Lipoid GmbH (Ludwigshafen, Germany) for providing LIPOID PC 18:0/18:0 and LIPOID PE 18:0/18:0. Furthermore, we would like to thank Annette Schucker for performing the XRD measurements of the dispersions.

Conflicts of Interest: The authors declare no conflict of interest.

Appendix A

Table A1. Composition of commercially available lecithins according to the manufacturer's specification (Lipoid GmbH, Ludwigshafen, Germany). n. sp. = not specified.

Components [%]	LIPOID PC 18:0/18:0	LIPOID PE 18:0/18:0
Phosphatidylcholine	≥99.0	n. sp.
Phosphatidylethanolamine	n. sp.	≥98.0
Lysophospholipids	≤0.5	≤0.5
Triacylglycerols	≤0.3	≤0.3
C16:0	n. sp.	n. sp.
C18:0	≥98.0	min. 98.0
Source	Synthetic	Synthetic

References

1. Müller, R.H.; Shegokar, R.; Keck, C.M. 20 years of lipid nanoparticles (SLN and NLC): Present state of development and industrial applications. *Curr. Drug Discov. Technol.* **2011**, *8*, 207–227. [CrossRef]
2. Müller, R.H.; Petersen, R.D.; Hommoss, A.; Pardeike, J. Nanostructured lipid carriers (NLC) in cosmetic dermal products. *Adv. Drug Deliv. Rev.* **2007**, *59*, 522–530. [CrossRef]
3. Pardeike, J.; Hommoss, A.; Müller, R.H. Lipid nanoparticles (SLN, NLC) in cosmetic and pharmaceutical dermal products. *Int. J. Pharm.* **2009**, *366*, 170–184. [CrossRef]
4. McClements, D.J. Crystals and crystallization in oil-in-water emulsions: Implications for emulsion-based delivery systems. *Adv. Colloid Interface Sci.* **2012**, *174*, 1–30. [CrossRef]
5. Dickinson, E.; Euston, S.R.; Woskett, C.M. Competitive adsorption of food macromolecules and surfactants at the oil-water interface. In *Surfactants and Macromolecules: Self-Assembly at Interfaces and in Bulk*; Lindman, B., Rosenholm, J.B., Stenius, P., Eds.; Steinkopff: Darmstadt, Germany, 1990; pp. 65–75. ISBN 978-3-7985-0838-5.
6. Mulder, H.; Walstra, P. *The Milk Fat Globule*; Commonwealth Agricultural Bureaux Farnham Royal: Buckinghamshire, UK, 1974; ISBN 0851982891.
7. McClements, D.J. *Food Emulsions*; CRC Press: Boca Raton, FL, USA, 2004; ISBN 9780429123894.
8. Boode, K.; Walstra, P. Partial coalescence in oil-in-water emulsions 1. Nature of the aggregation. *Colloids Surf. A Physicochem. Eng. Asp.* **1993**, *81*, 121–137. [CrossRef]
9. Awad, T.S.; Helgason, T.; Kristbergsson, K.; Decker, E.A.; Weiss, J.; McClements, D.J. Effect of Cooling and Heating Rates on Polymorphic Transformations and Gelation of Tripalmitin Solid Lipid Nanoparticle (SLN) Suspensions. *Food Biophys.* **2008**, *3*, 155–162. [CrossRef]
10. Walstra, P. Overview of Emulsion and Foam Stability. In *Food Emulsions and Foams: Interfaces, Interactions and Stability*; Dickinson, E., Ed.; Woodhead Publishing Ltd: Cambridge, UK, 1987; pp. 242–257. ISBN 978-1-85573-785-3.
11. Vanapalli, S.A.; Palanuwech, J.; Coupland, J.N. Stability of emulsions to dispersed phase crystallization: Effect of oil type, dispersed phase volume fraction, and cooling rate. *Colloids Surf. A Physicochem. Eng. Asp.* **2002**, *204*, 227–237. [CrossRef]
12. Bunjes, H.; Westesen, K.; Koch, M.H.J. Crystallization tendency and polymorphic transitions in triglyceride nanoparticles. *Int. J. Pharm.* **1996**, *129*, 159–173. [CrossRef]
13. Di Bari, V.; Macnaughtan, W.; Norton, J.; Sullo, A.; Norton, I. Crystallisation in water-in-cocoa butter emulsions: Role of the dispersed phase on fat crystallisation and polymorphic transition. *Food Struct.* **2017**, *12*, 82–93. [CrossRef]
14. Fredrick, E.; Walstra, P.; Dewettinck, K. Factors governing partial coalescence in oil-in-water emulsions. *Adv. Colloid Interface Sci.* **2010**, *153*, 30–42. [CrossRef]
15. Goibier, L.; Lecomte, S.; Leal-Calderon, F.; Faure, C. The effect of surfactant crystallization on partial coalescence in O/W emulsions. *J. Colloid Interface Sci.* **2017**, *500*, 304–314. [CrossRef] [PubMed]
16. Reiner, J.; Ly, T.T.; Liu, L.; Karbstein, H.P. Melt Emulsions: Influence of the Cooling Procedure on Crystallization and Recrystallization of Emulsion Droplets and their Influence on Dispersion Viscosity upon Storage. *Chem.-Ing.-Tech.* **2022**, *94*, 356–364. [CrossRef]
17. Beverung, C.J.; Radke, C.J.; Blanch, H.W. Protein adsorption at the oil/water interface: Characterization of adsorption kinetics by dynamic interfacial tension measurements. *Biophys. Chem.* **1999**, *81*, 59–80. [CrossRef] [PubMed]
18. Bergfreund, J.; Bertsch, P.; Fischer, P. Adsorption of proteins to fluid interfaces: Role of the hydrophobic subphase. *J. Colloid Interface Sci.* **2021**, *584*, 411–417. [CrossRef]
19. Mitropoulos, V.; Mütze, A.; Fischer, P. Mechanical properties of protein adsorption layers at the air/water and oil/water interface: A comparison in light of the thermodynamical stability of proteins. *Adv. Colloid Interface Sci.* **2014**, *206*, 195–206. [CrossRef]
20. Bos, M.A.; van Vliet, T. Interfacial rheological properties of adsorbed protein layers and surfactants: A review. *Adv. Colloid Interface Sci.* **2001**, *91*, 437–471. [CrossRef]
21. Heiden-Hecht, T.; Drusch, S. Impact of Saturation of Fatty Acids of Phosphatidylcholine and Oil Phase on Properties of β-Lactoglobulin at the Oil/Water Interface. *Food Biophys.* **2022**, *17*, 171–180. [CrossRef]
22. Coultate, T.P. *FOOD The Chemistry of Its Components*, 4th ed.; Royal Society of Chemistry: Cambridge, UK, 2002; ISBN 978-0-85404-615-7.
23. Karbstein, H.; Schubert, H. Developments in the continuous mechanical production of oil-in-water macro-emulsions. *Chem. Eng. Process. Process Intensif.* **1995**, *34*, 205–211. [CrossRef]
24. Karbstein, H.; Schubert, H. Einflußparameter auf die Auswahl einer Maschine zum Erzeugen feindisperser O/W-Emulsionen. *Chem.-Ing.-Tech.* **1995**, *67*, 616–619. [CrossRef]
25. Stang, M.; Karbstein, H.; Schubert, H. Adsorption kinetics of emulsifiers at oil—Water interfaces and their effect on mechanical emulsification. *Chem. Eng. Process. Process Intensif.* **1994**, *33*, 307–311. [CrossRef]
26. Heiden-Hecht, T.; Taboada, M.L.; Brückner-Gühmann, M.; Karbstein, H.P.; Gaukel, V.; Drusch, S. Towards an improved understanding of spray-dried emulsions: Impact of the emulsifying constituent combination on characteristics and storage stability. *Int. Dairy J.* **2021**, *121*, 105134. [CrossRef]
27. Bylaite, E.; Nylander, T.; Venskutonis, R.; Jönsson, B. Emulsification of caraway essential oil in water by lecithin and beta-lactoglobulin: Emulsion stability and properties of the formed oil-aqueous interface. *Colloids Surf. B Biointerfaces* **2001**, *20*, 327–340. [CrossRef] [PubMed]

28. Fang, Y.; Dalgleish, D.G. Comparison of the effects of three different phosphatidylcholines on casein-stabilized oil-in-water emulsions. *J. Am. Oil Chem. Soc.* **1996**, *73*, 437–442. [CrossRef]
29. Fang, Y.; Dalgleish, D.G. *Interactions between Sodium Caseinate and Dioleoylphosphatidylcholine on Oil–Water Interfaces and in Solution. Food Colloids*; Elsevier: Amsterdam, The Netherlands, 2004; pp. 67–76. ISBN 9781855737839.
30. McClements, D.J.; Dungan, S.R.; German, J.B.; Simoneau, C.; Kinsella, J.E. Droplet Size and Emulsifier Type Affect Crystallization and Melting of Hydrocarbon-in-Water Emulsions. *J. Food Sci.* **1993**, *58*, 1148–1151. [CrossRef]
31. Bunjes, H.; Koch, M.H.J. Saturated phospholipids promote crystallization but slow down polymorphic transitions in triglyceride nanoparticles. *J. Control Release* **2005**, *107*, 229–243. [CrossRef]
32. Günther, E.; Schmid, T.; Mehling, H.; Hiebler, S.; Huang, L. Subcooling in hexadecane emulsions. *Int. J. Refrig.* **2010**, *33*, 1605–1611. [CrossRef]
33. Abramov, S.; Ahammou, A.; Karbstein, H.P. Influence of external forces during supercooling on dispersion stability during melt emulsification. *Chem. Eng. Technol.* **2018**, *41*, 768–775. [CrossRef]
34. Abramov, S.; Shah, K.; Weißenstein, L.; Karbstein, H. Effect of Alkane Chain Length on Crystallization in Emulsions during Supercooling in Quiescent Systems and under Mechanical Stress. *Processes* **2018**, *6*, 6. [CrossRef]
35. Bayard, M.; Cansell, M.; Leal-Calderon, F. Crystallization of emulsified anhydrous milk fat: The role of confinement and of minor compounds. A DSC study. *Food Chem.* **2022**, *373*, 131605. [CrossRef] [PubMed]
36. Palanuwech, J.; Coupland, J.N. Effect of surfactant type on the stability of oil-in-water emulsions to dispersed phase crystallization. *Colloids Surf. A Physicochem. Eng. Asp.* **2003**, *223*, 251–262. [CrossRef]
37. Awad, T.; Sato, K. Acceleration of crystallisation of palm kernel oil in oil-in-water emulsion by hydrophobic emulsifier additives. *Colloids and Surfaces B: Biointerfaces* **2002**, *25*, 45–53. [CrossRef]
38. Truong, T.; Bansal, N.; Sharma, R.; Palmer, M.; Bhandari, B. Effects of emulsion droplet sizes on the crystallisation of milk fat. *Food Chem.* **2014**, *145*, 725–735. [CrossRef]
39. Relkin, P.; Sourdet, S.; Fosseux, P.-Y. Fat crystallization in complex food emulsions: Effects of adsorbed milk proteins and of a whipping process. *J. Therm. Anal. Calorim.* **2003**, *71*, 187–195. [CrossRef]
40. Garti, N.; Sato, K. *Crystallization and Polymorphism of Fats and Fatty Acids*; Marcel Dekker: New York, NY, USA, 1988.
41. Larsson, K. Classification of glyceride crystal forms. *Acta Chem. Scand.* **1966**, *20*, 2255–2260. [CrossRef]
42. Himawan, C.; Starov, V.M.; Stapley, A.G.F. Thermodynamic and kinetic aspects of fat crystallization. *Adv. Colloid Interface Sci.* **2006**, *122*, 3–33. [CrossRef] [PubMed]
43. Sato, K.; Ueno, S.; Yano, J. Molecular interactions and kinetic properties of fats. *Prog. Lipid Res.* **1999**, *38*, 91–116. [CrossRef]
44. Gunstone, F. *The Chemistriy of Oils and Fats: Sources, Composition, Properties and Uses*; John Wiley & Sons: Hoboken, NJ, USA, 2009.
45. Acevedo, N.C.; Marangoni, A.G. Functionalization of Non-interesterified Mixtures of Fully Hydrogenated Fats Using Shear Processing. *Food Bioprocess Technol.* **2014**, *7*, 575–587. [CrossRef]
46. Marangoni, A.G.; McGauley, S.E. Relationship between Crystallization Behavior and Structure in Cocoa Butter. *Cryst. Growth Des.* **2003**, *3*, 95–108. [CrossRef]
47. Chapman, G.M.; Akehurst, E.E.; Wright, W.B. Cocoa butter and confectionery fats. Studies using programmed temperature X-ray diffraction and differential scanning calorimetry. *J. Am. Oil Chem. Soc.* **1971**, *48*, 824–830. [CrossRef]
48. Reiner, J.; Peyronel, F.; Weiss, J.; Marangoni, A.G. Monitoring the Polymorphic Transformation of a Palm Kernel-Based Emulsion Using Ultrasound. *Food Bioprocess Technol.* **2018**, *11*, 797–808. [CrossRef]
49. Lopez, C.; Bourgaux, C.; Lesieur, P.; Ollivon, M. Coupling of time-resolved synchrotron X-ray diffraction and DSC to elucidate the crystallisation properties and polymorphism of triglycerides in milk fat globules. *Lait* **2007**, *87*, 459–480. [CrossRef]
50. Westesen, K.; Siekmann, B.; Koch, M.H.J. Investigations on the physical state of lipid nanoparticles by synchrotron radiation X-ray diffraction. *Int. J. Pharm.* **1993**, *93*, 189–199. [CrossRef]
51. Siekmann, B.; Westesen, K. Thermoanalysis of the recrystallization process of melt-homogenized glyceride nanoparticles. *Colloids Surf. B Biointerfaces* **1994**, *3*, 159–175. [CrossRef]
52. Arbeitsgemeinschaft für Pharmazeutische Verfahrenstechnik; Association de Pharmacie Galénique Industrielle. Complex Fats as Matrix Constitutions in Lipid Nanoparticles. In Proceedings of the 1st World Meeting of APGI/APV, Budapest, Hungary, 9–11 May 1995.
53. Bunjes, H.; Koch, M.H.J.; Westesen, K. Effect of Particle Size on Colloidal Solid Triglycerides. *Langmuir* **2000**, *16*, 5234–5241. [CrossRef]
54. Bunjes, H.; Koch, M.H.J.; Westesen, K. Effects of surfactants on the crystallization and polymorphism of lipid nanoparticles. In *Molecular Organisation on Interfaces*; Lagaly, G., Ed.; Springer: Berlin, Heidelberg, 2006; pp. 7–10. ISBN 978-3-540-43637-9.
55. Aronhime, J.S.; Sarig, S.; Garti, N. Dynamic control of polymorphic transformation in triglycerides by surfactants: The button syndrome. *J. Am. Oil Chem. Soc.* **1988**, *65*, 1144–1150. [CrossRef]
56. Bunjes, H.; Koch, M.H.J.; Westesen, K. Influence of emulsifiers on the crystallization of solid lipid nanoparticles. *J. Pharm. Sci.* **2003**, *92*, 1509–1520. [CrossRef] [PubMed]
57. Gordillo-Galeano, A.; Mora-Huertas, C.E. Solid lipid nanoparticles and nanostructured lipid carriers: A review emphasizing on particle structure and drug release. *Eur. J. Pharm. Biopharm.* **2018**, *133*, 285–308. [CrossRef] [PubMed]
58. Tippetts, M.; Martini, S. Effect of cooling rate on lipid crystallization in oil-in-water emulsions. *Food Res. Int.* **2009**, *42*, 847–855. [CrossRef]

59. Salminen, H.; Helgason, T.; Aulbach, S.; Kristinsson, B.; Kristbergsson, K.; Weiss, J. Influence of co-surfactants on crystallization and stability of solid lipid nanoparticles. *J. Colloid Interface Sci.* **2014**, *426*, 256–263. [CrossRef] [PubMed]
60. Zhang, N.; Liu, C.; Jin, L.; Zhang, R.; Siebert, H.-C.; Wang, Z.; Prakash, S.; Yin, X.; Li, J.; Hou, D.; et al. Influence of Long-Chain/Medium-Chain Triglycerides and Whey Protein/Tween 80 Ratio on the Stability of Phosphatidylserine Emulsions (O/W). *ACS Omega* **2020**, *5*, 7792–7801. [CrossRef]
61. Romo-Uribe, A. Wide-angle X-ray diffraction and small-angle X-ray scattering studies of elastomer blends and composites. In *Elastomer Blends and Composites*; Elsevier: Amsterdam, The Netherlands, 2022; pp. 209–242. ISBN 9780323858328.
62. D'Souza, V.; deMan, J.M.; deMan, L. Short spacings and polymorphic forms of natural and commercial solid fats: A review. *J. Am. Oil Chem. Soc.* **1990**, *67*, 835–843. [CrossRef]
63. Mazzanti, G.; Guthrie, S.E.; Sirota, E.B.; Marangoni, A.G.; Idziak, S.H.J. Effect of Minor Components and Temperature Profiles on Polymorphism in Milk Fat. *Cryst. Growth Des.* **2004**, *4*, 1303–1309. [CrossRef]
64. Guttman, S.; Ocko, B.M.; Deutsch, M.; Sloutskin, E. From faceted vesicles to liquid icoshedra: Where topology and crystallography meet. *Curr. Opin. Colloid Interface Sci.* **2016**, *22*, 35–40. [CrossRef]
65. Cholakova, D.; Valkova, Z.; Tcholakova, S.; Denkov, N.; Smoukov, S.K. "Self-Shaping" of Multicomponent Drops. *Langmuir* **2017**, *33*, 5696–5706. [CrossRef] [PubMed]
66. Reiner, J.; Martin, D.; Ott, F.; Harnisch, L.; Gaukel, V.; Karbstein, H.P. Influence of the Triglyceride Composition, Surfactant Concentration and Time–Temperature Conditions on the Particle Morphology in Dispersions. *Colloids Interfaces* **2023**, *7*, 22. [CrossRef]
67. Robinson, C.D. Some factors influencing sedimentation. *Ind. Eng. Chem.* **1926**, *18*, 869–871. [CrossRef]
68. McClements, D.J.; Dungan, S.R.; German, J.B.; Kinsella, J.E. Factors which affect oil exchange between oil-in-water emulsion droplets stabilized by whey protein isolate: Protein concentration, droplet size and ethanol. *Colloids Surf. A Physicochem. Eng. Asp.* **1993**, *81*, 203–210. [CrossRef]
69. Helgason, T.; Awad, T.S.; Kristbergsson, K.; McCLEMENTS, D.J.; Weiss, J. Influence of Polymorphic Transformations on Gelation of Tripalmitin Solid Lipid Nanoparticle Suspensions. *J. Am. Oil Chem. Soc.* **2008**, *85*, 501–511. [CrossRef]
70. Samtlebe, M.; Yucel, U.; Weiss, J.; Coupland, J.N. Stability of Solid Lipid Nanoparticles in the Presence of Liquid Oil Emulsions. *J. Am. Oil Chem. Soc.* **2012**, *89*, 609–617. [CrossRef]
71. Helgason, T.; Awad, T.S.; Kristbergsson, K.; McClements, D.J.; Weiss, J. Effect of surfactant surface coverage on formation of solid lipid nanoparticles (SLN). *J. Colloid Interface Sci.* **2009**, *334*, 75–81. [CrossRef]
72. Johansson, D.; Bergenståhl, B. Sintering of fat crystal networks in oil during post-crystallization processes. *J. Am. Oil Chem. Soc.* **1995**, *72*, 911–920. [CrossRef]